Unsupported SiO_2-based organic–inorganic membranes

Part 2:† Surface features and gas permeation

Sandra Dirè,* Eva Pagani, Riccardo Ceccato and Giovanni Carturan

Dipartimento di Ingegneria dei Materiali, Università di Trento, v. Mesiano 77, 38050 Trento, Italy

Gas permeation of unsupported hybrid membranes, obtained by co-hydrolysis of various $Si(OEt)_4/MeSi(OEt)_3$ (TEOS/MTES) mixtures, is studied with Ar, He and N_2. The separation performance of these hybrid membranes is higher than for pure SiO_2 sol–gel derived membranes and depends on chemical composition: a considerable increase in separation factor $\alpha(He/N_2)$ is found as the amount of MTES increases; moreover, gas permeability decreases with increasing organic modification of the network. Membrane characterization is performed by N_2 adsorption–desorption measurements and low-temperature differential scanning calorimetry (DSC) and dynamic contact angle (DCA) analyses. Data are related to chemical composition, affecting both the chemical nature of the surface and gas permeation. Results indicate that gas permeation through hybrid membranes may favour the Knudsen flow model or surface diffusion mechanism, depending on the TEOS/MTES ratio.

The drawbacks of pure inorganic membranes are their brittleness and poor separation properties, partly offset by higher thermal stability, chemical durability and ease of generation.

While chemical composition affects the working of organic membranes, as triggered by solution-diffusion mechanisms,[1,2] the high permeability and low separation capacity of inorganic membranes are mainly related to the pore size distribution,[3,4] indicating that the disadvantages of inorganic membranes may be overcome by improving their synthesis.

Organic–inorganic hybrid materials are an optimal compromise between improvement in separation properties and maintenance of favourable permeability and thermal resistance.[5,6] One such improvement is the combination of narrow pore size distribution and good diffusion on the pore surface, *i.e.*, between the high permeability of porous inorganic membranes and the high selectivity of non-porous organic ones. Achieving this involves controlling the membrane surface in terms of pore availability and also polarity. This fact prompted us to study the gas permeation of SiO_2-based organic–inorganic membranes, considering the chemical nature of the exposed membrane surface which may account for the gas permeability mechanism, and identifying preparation conditions suitable for enhancing separation features.

In the first part of our research[7] we reported the preparation and structural characterization of unsupported SiO_2-based hybrid membranes prepared with various $Si(OEt)_4/MeSi(OEt)_3$ ratios. We report here our study on gas permeation, since we believe that this property is connected to the surface and porosity features which ultimately depend on chemical composition, *i.e.*, the $Si(OEt)_4/MeSi(OEt)_3$ ratio.

Experimental

Preparation of $Si(OEt)_4/MeSi(OEt)_3$ (TEOS/MTES, T/M) membranes was reported in Part 1.[7] Samples were labelled T*x*M*y*, where *x* and *y* represent the molar percentages of TEOS and MTES, respectively.

Surface area measurements and pore size distributions were obtained by nitrogen adsorption–desorption on samples degassed overnight at 80 °C on a Carlo Erba Sorptomatic 1800. The BET equation was linear in the interval $0.05 \leqslant p/p_0 \leqslant 0.33$, with a least-squares fit of 0.998 and *C* BET constant in the interval 5–10, for all compositions. Mercury intrusion porosimetry measurements were performed on a Carlo Erba Porosimeter 2000.

Differential scanning calorimetry (DSC) measurements were obtained on a Mettler TC 10A; 30 mg samples were put into sealed pans perforated with some pinholes to allow pressure equilibration, and heated at 10 °C min^{-1} from −50 to 150–300 °C. DSC scans were repeated to verify trend reproducibility. Actual temperatures corresponding to DSC effects were calculated by measuring the extrapolated onset temperatures with the software provided.

Dynamic contact angles (DCA) were obtained in water at 25 ± 2 °C on a Cahan microbalance using a procedure described elsewhere.[8] Samples 10–40 μm thick were cut into 1×1.5 cm pieces and treated under vacuum (10^{-3} Torr) for 24 h before advancing and receding contact angles were measured. Five independent measurements were averaged and the standard deviation was ± 3°.

Gas permeability was measured according to Darcy's law for porous materials, using a laboratory-built apparatus equipped with a membrane holder, a U-tube manometer to measure the pressure difference across the membrane, and a flowmeter to measure the gas flow rate across the membrane.[9] The apparatus was maintained at a constant temperature of 25 °C and checked before experiments with an applied pressure of 30 cmHg for 24 h. Permeability *Q* was calculated according to:

$$Q = (F\ t)/(\Delta P\ A) \quad (1)$$

where *Q* is expressed in barrers [1 barrer = 10^{-10} cm^3 (STP) cm cm^{-2} $(cmHg)^{-1}$ s^{-1}], *F* is the gas flow rate [10^{-10} cm^3 (STP) s^{-1}], *A* the membrane area (cm^2), ΔP the pressure drop (cmHg), and *t* the membrane thickness (cm). Measurements were carried out at 25 °C with chromatographic-grade He, N_2 and Ar. Data were averaged over 5 independent measurements. Separation factors α were expressed as the ratio between the permeabilities of the various gases.[9]

Results

N_2 adsorption–desorption

Specific surface areas and pore size distributions were calculated by means of Brunauer, Emmett, Teller (BET) and Kelvin equations, respectively. As adsorbed volume *vs.* p/p_0 plots are rather difficult to compare with the standard isotherms of the

†Part 1: ref. 7.

Brunauer[10] classification and hysteresis loops cannot give conclusive information regarding pore shape definition, pore size calculations were based on the cylindrical model, according to the synthesis conditions.[11] All samples had low specific surface areas, from 45 $m^2\ g^{-1}$ for T100 to 20 $m^2\ g^{-1}$ for M100. Sorption capacity ranged between 80 and 9 $cm^3\ g^{-1}$ for T100 and M100, respectively, with pore volumes ranging from 0.03 $cm^3\ g^{-1}$ for M100 and 0.13 $cm^3\ g^{-1}$ for T100. Fig. 1 shows a typical pore size distribution, with a peak below 20 Å and no pores with radii >100 Å. This trend was confirmed by mercury intrusion porosimetry, which excluded the presence of pore radii >300 Å. As the amount of MTES increased, no important porosity changes were observed, due to the negligible changes of specific surface areas, the main effect being lower pore size distribution with progressive reduction of high-radius pores. This fact is evident from the plot of porosity *vs.* radius of various samples (Fig. 2).

DSC and DCA results

DSC and DCA analyses are performed on samples stored for almost four months at constant temperature and humidity, assuring a steady state of aging. Fig. 3(*a*) shows the T100 DSC diagram, with a strong endothermal band centred at 84 °C. This effect was also present for other TxM*y* samples having $x \neq 0$. The M100 DSC curve of Fig. 3(*b*) shows a glass transition at 37 °C, without other effects. Table 1 summarizes our DSC results: both endothermal band intensity and temperature appear to depend closely on the percentage of MTES, since the calculated ΔH values became smaller and the effect was observed at higher temperatures as MTES increased.

The DSC diagrams showed endothermal effects with increased intensities as exposure time increased when samples were exposed to the atmosphere for consecutive runs (Table 2). When contact with the atmosphere was prevented after the first measurement, the effect on T100 showed a strong decrease in intensity (Table 2).

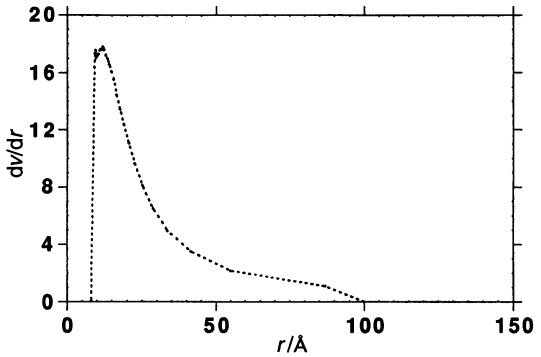

Fig. 1 Pore size distribution of T100 membrane calculated from N_2 adsorption–desorption isotherms

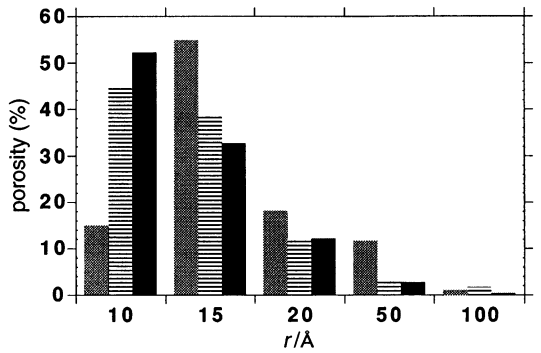

Fig. 2 Comparison between pore size distributions of TxM*y* membranes. T100 (grey), T70M30 (stripes), T50M50 (black).

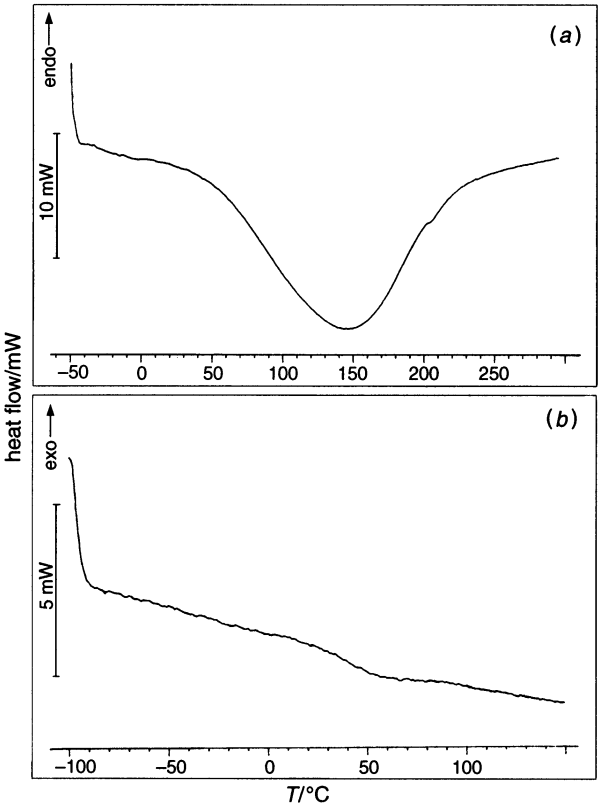

Fig. 3 DSC curves of (*a*) T100 and (*b*) M100 membranes. The endothermal band in (*a*) is attributed to the boiling of water in pores; in (*b*) the inflection point corresponds to the glass transition.

Table 1 Position and intensity of the DSC endothermal band

sample	ΔH/J g^{-1}	T/°C
T100	272.9	84
T70M30	179.6	90
T50M50	139.3	93
T30M70	37.3	93

Table 2 Dependence of DSC endothermal band intensity upon exposure to atmosphere

exposure time/h	run 1, ΔH/J g^{-1}	run 2, ΔH/J g^{-1}
0	272.9	1.7
2.5	272.9	52.6
24	272.9	116.4

Fig. 4 shows DCA results obtained with water at 25 °C. Sample wettability decreased as MTES % increased, concomitant with the highest advancing contact angle of M100. The same behaviour was found for receding angles, although they were always lower than advancing ones. This hysteresis, commonly attributed to surface roughness,[12] may also be affected by water contamination of the surface after dipping.

Gas permeation

Gas permeation was studied with He, N_2 and Ar. Fig. 5 shows that N_2 permeability depends on applied pressure and also indicates He and Ar trends. Permeability at 25 °C was high at low pressures, falling to a plateau after 15 cmHg. To prevent effects derived from starting up, contamination by other gases, and preferential interaction with the surface occurring at low pressures, the permeability data of Table 3 are calculated at $\Delta P = 20$ cmHg. Permeability decreased as MTES content increased. The permeability of sample T100 is comparable with

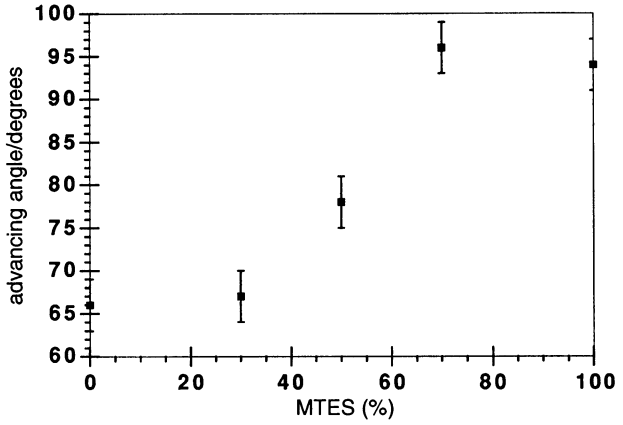

Fig. 4 Wettability of T*x*M*y* membranes, measured by the DCA technique, *vs.* chemical composition

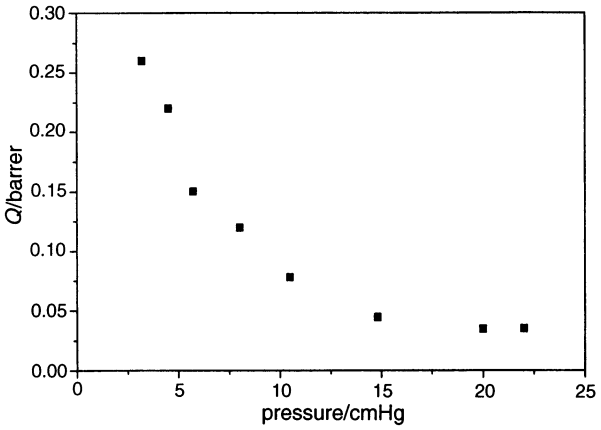

Fig. 5 Calculated N_2 permeabilities ($\times 10^5$) of T100 membrane at room temperature as a function of applied pressure

Table 3 Gas permeation performances

sample	Q_{Ar}[a]/ barrer	Q_{N_2}[a]/ barrer	Q_{He}[a]/ barrer	$\alpha(He/N_2)$	$\alpha(N_2/Ar)$
T100	3000	3500	17000	4.8	1.16
T70M30	1300	1400	15000	10.4	1.12
T50M50	420	490	11000	23.0	1.16
T30M70	410	500	9400	18.8	1.21
M100	250	290	6500	22.5	1.16

[a]Estimated error on calculated permeability = 5%.

that reported for microporous silica;[13] M100 shows behaviour similar to that of polydimethylsiloxane.[14] For all compositions, separation factor α, calculated as reported in the Experimental section, was quite high in the case of He–N_2 and was greater than the Knudsen flow value 2.6.[14] Although the α values of modified samples strongly increased for T*x*M*y* membranes, a linear relationship with composition cannot be proposed. Instead, the N_2/Ar ratio did not depend on MTES % and fitted the Knudsen value of 1.2.

Discussion

Homogeneous and transparent unsupported membranes were successfully prepared from pure TEOS and MTES mixtures, the hydrolysis–condensation process being performed with a low water/silane ratio, in acid conditions.[7] These membranes appear to be dense and homogeneous to scanning electron microscopy, atomic force microscopy analysis revealing a characteristic surface waviness.[8]

Pore size distributions (Fig. 2) show that the increase in methyl content fitted the observed narrowing in pore size distribution: pores with a 10 Å radius increased, whereas pores with $r \geqslant 50$ Å progressively disappeared. The plot of layer thickness as a function of volume adsorbed, *t*-plot,[15] indicated that the T*x*M*y* samples may be described as microporous solids. In spite of their porosity features, the membranes had low specific surface areas: 45 $m^2\ g^{-1}$ for T100 and 20 $m^2\ g^{-1}$ for M100. The *C* BET values were also low, suggesting weak or difficult adsorbent–adsorbate interactions.[16] Exceedingly low surface areas were unusual,[5,17] although Avnir and co-workers[18] recently demonstrated that the apparently low surface areas obtained by N_2 sorption could be incorrect in the case of microporous sol–gel materials, due to the extreme slowness of nitrogen diffusion through the micropores. This effect was particularly notable in sol–gel derived SiO_2 prepared in acid conditions with a low water/silicon alkoxide ratio. The observed low surface area of our T*x*M*y* membranes may have a similar explanation.

An alternative possibility, deduced from sorption capacity values, is that low surface areas arise from low open pore availability: comparison of bulk and apparent densities gave 5% open porosity for T50M50. Preliminary SAXS results on M100, T50M50 and T100 xerogels also indicated the presence of an almost dense structure.

Introduction of Si–CH_3 groups into a SiO_2 gel network may account for pore distribution narrowing if the change in porosity is related to preferential silica surface coverage by methyl groups as Si–CH_3 group concentration increases. Indeed, Hua and Smith[19] reported that silylation of silica surfaces causes a decrease in surface area, with the disappearance of the largest pores.

Our DCA and DSC results support the above hypothesis. When the methyl content of the T*x*M*y* membranes was increased, wettability and water sorption ability decreased, as expected for progressive coverage of the silica surface by methyl groups. The relationships among water contact angle, Si–CH_3 content (Fig. 4) and decrease in DSC endothermal effect (Table 1) are noteworthy. The last of these depends on exposure time (Table 2), so that it is related to the release of surface water by boiling, resulting in a minor effect as the Si–CH_3 group concentration increases or wettability decreases. In addition, according to Wallace and Hench,[20] the slight increase in onset temperature of the DSC band as the percentage of MTES increases may be related to narrowing of the pore size distributions (Fig. 2). The absence of a detectable endothermal effect in the case of M100 [Fig. 3(*b*)] confirms that the surface of M100 is a dense arrangement of methyl groups.[8]

The permeability of T100 (Table 3) may be compared with results obtained by Klein *et al.*[13] on TEOS-derived unsupported membranes: 13100 and 6900 barrers for He and N_2 respectively, for membranes with pore sizes in the range 8–18 nm. In our case, pore distribution was concentrated on the smaller pore radii, accounting for the fall in permeation values. He, N_2 and Ar permeabilities (Table 3) were inversely dependent on the Si–CH_3 load into the SiO_2 gel network, apparently due to the observed decrease in surface area. However, in agreement with the findings of Okui *et al.*[21] on phenyl-substituted silica membranes, the separation factors of Table 3 indicate that gas permeation was more directly affected by gas *vs.* surface interactions than by flow through a porous medium: $\alpha(He/N_2)$ was always higher than the separation factor calculated assuming a Knudsen flow and increased with Si–CH_3 concentration, according to lowered nitrogen diffusion capability.

Gas transport through non-porous polymeric membranes is traditionally described by the dual mode sorption[22] and free volume[23] theories. The former is based on gas adsorption–desorption equilibria taking place in microcavities in the polymer matrix; the latter correlates diffusivity with the poly-

mer-free volume which, to a great extent, is related to chain mobility. The existence of a microstructure able to discriminate on a molecular level has a considerable effect on selectivity: thus, rigid glassy polymers usually have higher separation factors than rubbery materials, and this behaviour is associated with high permeability when bulky groups creating high free volumes are present in the polymers.[24]

Thus, N_2 diffusion in T*x*M*y* membranes may be limited not only by reduced adsorption–desorption ability. The network rigidity of our membranes increased with TEOS %, due to the close proximity of TEOS (Q) and MTES (T) derived units.[7] Thus, the $\alpha(He/N_2)$ and permeability values found for intermediate compositions may be related to the presence of methyl groups inside a poorly mobile network.

Instead, when non-porous and porous materials are used in composite membranes, Knudsen flow may contribute to the total flow, depending on pore size.[14] The permeability behaviour of our membranes towards Ar was comparable to that observed in the case of N_2, the N_2/Ar separation factor being close to the calculated Knudsen flow value. In this case, the close similarity in the polarizability and molecular size of N_2 and Ar may explain their similar behaviour, although the porosity effect prevails over surface diffusion limitations, indirectly supporting the above hypothesis.

In conclusion, gas permeation of hybrid materials is affected by the relative ratios of organic and inorganic moieties in the network. Gas transport mechanisms in porous and non-porous membranes should therefore both be taken into account in an effort to give a complete description of the phenomenum.

The authors acknowledge C. Gavazza for DSC measurements and C. Della Volpe for DCA measurements. E. Pagani thanks the Provincia Autonoma di Trento for financial support. The authors are grateful to Professor Paolo Giordano Orsini (died on July 28 1996) for his generous and untiring work at the University of Trento.

References

1 T. Graham, *Philos. Mag*., 1866, **32**, 401.
2 P. Meares, in *Membranes in Gas Separation and Enrichment*, ed. A. Williams, The Royal Society of Chemistry, London, 1986, pp. 1–25.
3 K. Keizer, R. J. R. Uhlhorn, R. J. Van Vuren and A. J. Burggraaf, *J. Membr. Sci*., 1988, **39**, 285.
4 W. F. Maier, I. Tilgner, M. Wiedorn, H. Ko, A. Ziehfreund and R. Sell, *Adv. Mater*.,1993, **5**, 730.
5 A. Kaiser, H. Schmidt and H. Bottner, *J. Membr. Sci*., 1985, **22**, 257.
6 (*a*) C. Guizard, N. Ajaka, M. P. Besland, A. Larbot and L. Cot, in *Polyimides and Other High Temperature Polymers*, ed. M. K. M. Abadie and B. Sillion, Elsevier Science, Amsterdam, 1991, p. 537; (*b*) C. Guizard and P. Lacan, in *Proceedings of First European Workshop on Hybrid Organic Inorganic Materials*, Bierville, November 8–10, 1993, ed. C. Sanchez and F. Ribot, CNRS, Paris, 1993, p. 153.
7 S. Dirè, E. Pagani, F. Babonneau, R. Ceccato and G. Carturan, *J. Mater. Chem*., 1997, **7**, 67.
8 C. Della Volpe, S. Dirè and E. Pagani, *J. Non-Cryst. Solids*, 1997, **209**, 51.
9 L. C. Klein and N. Giszpenc, *Ceram. Bull*., 1990, **69**, 1821.
10 S. Brunauer, P. H. Emmett and E. Teller, *J. Am. Chem. Soc*., 1938, **60**, 309.
11 J. F. Quinson, J. Dumas and J. Serughetti, *J. Non-Cryst. Solids,* 1986, **79**, 397.
12 R. J. Good, *J. Am. Chem. Soc*., 1952, **74**, 5041.
13 L. C. Klein, T. Bloxom and R. Woodman, *Colloids Surf*., 1992, **63**, 173.
14 M. Mulder, *Basic Principles of Membrane Technology*, Kluwer Academic, Dordrecht, Netherlands, 1991, ch. 5.
15 B. C. Lippens and J. H. de Boer, *J. Catal*., 1965, **4**, 319.
16 S. J. Gregg and K. S. W. Sing, *Adsorption, Surface Area and Porosity*, Academic Press, London, 1982, ch. 2.
17 K. G. Sharp, *J. Sol–Gel Sci. Technol*., 1994, **2**, 35.
18 Y. Polevaya, J. Samuel, M. Ottolenghi and D. Avnir, *J. Sol–Gel Sci. Technol*., 1995, **5**, 65.
19 D. Hua, and D. M. Smith, *Mater. Res. Soc. Symp. Proc*., 1992, **271**, 547.
20 S. Wallace and L. L. Hench, *J. Sol–Gel Sci. Technol*., 1994, **1**, 153.
21 T. Okui, Y. Saito, T. Okubo and M. Sadakata, *J. Sol–Gel Sci. Technol*., 1995, **5**, 127.
22 W. R. Vieth and J. M. Howell, *J. Membr. Sci*., 1976, **1**, 177.
23 H. Fujita, *Fortschr. Hochpolym. Forsch*. 1961, **3**, 1.
24 E. R. Hensema, *Adv. Mater*., 1994, **6**, 269 and references therein.

Paper 6/08382J; *Received* 13*th December*, 1996